Journal of Energy Storage 63 (2023) 107001

Contents lists available at ScienceDirect

Journal of Energy Storage

journal homepage: www.elsevier.com/locate/est

Research Papers

Thermal energy storage optimization using composite foam-nano enhanced phase change materials

Mehdi Ghalambaz [a,b], Mutabe Aljaghtham [c], Mehdi Fteiti [d], Ali J. Chamkha [e], Abdelkader Abdullah [c,f], Mohammad Ghalambaz [g,*]

[a] Institute of Research and Development, Duy Tan University, Da Nang 550000, Viet Nam
[b] Faculty of Electrical – Electronic Engineering, Duy Tan University, Da Nang 550000, Viet Nam
[c] Department of Mechanical Engineering, College of Engineering in Al-Kharj, Prince Sattam Bin Abdulaziz University, Al-Kharj 11942, Saudi Arabia
[d] Physics Department, Faculty of Applied Science, Umm Al-Qura University, Makkah 24381, Saudi Arabia
[e] Faculty of Engineering, Kuwait College of Science and Technology, Doha District 35004, Kuwait
[f] Mechanical Power Engineering Department, Faculty of Engineering, Tanta University, Tanta 31521, Egypt
[g] Laboratory on Convective Heat and Mass Transfer, Tomsk State University, 634045 Tomsk, Russia

ARTICLE INFO

Keywords:
Open thermal energy storage unit
Metal foam
Nano-enhanced phase change materials
Latent heat thermal energy storage

ABSTRACT

A design of latent heat thermal energy storage (LHTES) unit for the rapid charging process of the nano-enhanced coconut oil inside an open-cell copper foam was proposed. A stream of hot liquid coconut oil was allowed to enter the thermal energy storage unit from the bottom and leave the unit from the top to accelerate the melting process. A heat transfer tube was placed inside the unit to melt the PCM layer and open a liquid film passage between the inlet and the outlet. The impact of design parameters such as porosity of copper foam, inlet PCM liquid pressure, hot inlet liquid inside the heat transfer tube, and volume fractions of nanoparticles was investigated on the charging time of the unit and its thermal behavior. The formation of the liquid PCM film over the heated tube is the key to fast charging. The key parameter in liquid film formation was the inlet velocity of hot liquid inside the tube. Increasing the inlet velocity by 2.5 times could reduce the thermal charging time by 2.5 times. Moreover, using nano-additives was not beneficial in this design since they could delay the liquid PCM film formation and the charging time.

1. Introduction

Renewable energy seems to have become increasingly popular, not just to decrease energy use but also to mitigate environmental damage. However, because of the fluctuations in renewable energy production, these technologies mismatch the energy supply with the energy load demand [1]. Energy storage systems (ESSs) are invented to overcome this issue [2]. Thermal energy storage (TES) is one of these useful ESS, which has encouraged various scientists to concentrate on TES. In addition to its employment in renewable energy, TES is currently used in multiple applications, such as healthcare, building materials, aerospace, and refrigerants [3]. In recent years, phase change materials (PCMs) have attracted much interest as an alternative to existing thermal storage approaches [4,5]. Some researchers also introduced by-product of the non-metallic industry as inorganic PCMs [6,7]. Electronic components and batteries also produce a notable amount of energy [8,9], and thus PCMs have been proposed for thermal management [10].

When the ambient temperature is near PCM's fusion temperature, it absorbs or releases energy through melting or solidification. Low thermal conductivity and thermal diffusion in the bulk PCM act as barriers, delaying the heat transfer and lowering the overall efficiency [11]. The limited heat conductivity of PCMs makes the complete deployment of these systems for everyday life applications impractical [12]. To tackle this problem, either a higher PCM mass is used, which results in a higher cost and volume, which is undesirable, or heat transfer enhancement techniques are used [13]. Various approaches have been proposed for this purpose, including the use of encapsulated PCM [14], a more complicated heat exchanger structure [15], adding highly conductive nanoparticles [16], and the most current option, the use of a conductive porous medium [17,18]. Moreover, nano-additives and phase change mechanisms have been proposed as heat transfer enhancers for cooling liquids in microchannel heatsinks [19,20].

* Corresponding author.
E-mail addresses: mehdighalambaz@duytan.edu.vn (M. Ghalambaz), m.ghalambaz@gmail.com (M. Ghalambaz).

https://doi.org/10.1016/j.est.2023.107001
Received 17 October 2022; Received in revised form 20 December 2022; Accepted 25 February 2023
Available online 21 March 2023

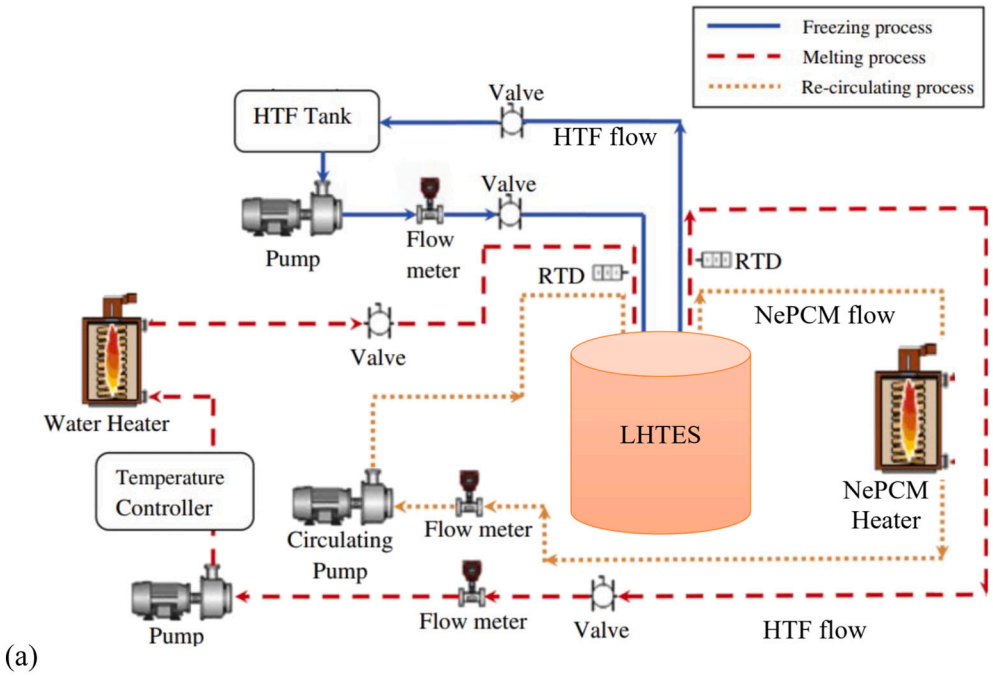

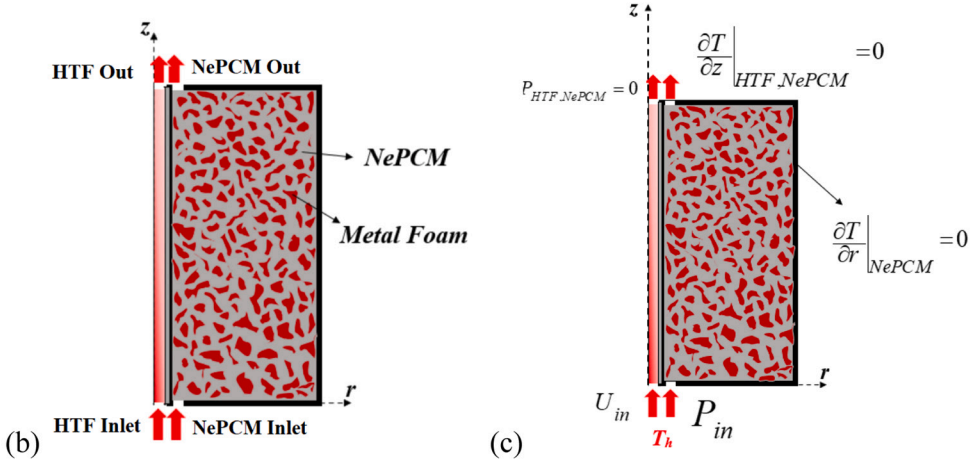

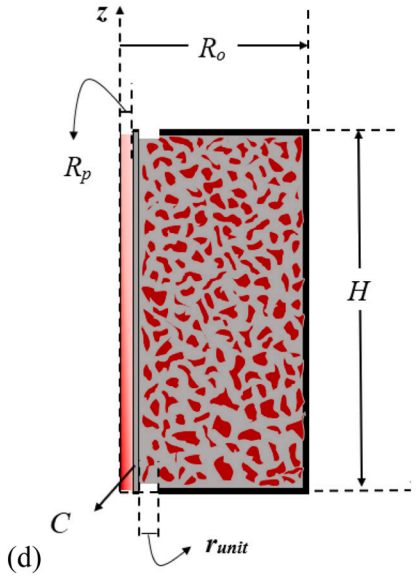

Fig. 1. Thermodynamic cycle for dynamic melting. The thermodynamic cycle with some modifications was taken from [28]. There are two heating (charging) cycles and one cooling (discharging cycle). The HTF flows inside the tube and is not in direct contact with NePCM. The NePCM enters and leaves the shell side in a heating cycle. The cooling cycle takes place just by HTF flow. The schematic diagram of the physical model is illustrated in (b) model description, (c) boundary conditions, and (d) geometrical parameters.

While some strategies have been discovered to be quite efficient at enhancing heat transfer, they are intrusive because a less amount of PCM could be implanted within the Latent Heat TES (LHTES) set. As a result, the ratio of PCM volume to the volume of the LHTES system decreases, as does the energy storage capacity. Researchers concentrated on heat transfer without invasiveness augmentation techniques such as dynamic PCM systems, direct contact PCM structures, and PCM slurries [21,22]. The dynamic PCM systems operate based on the PCM moving or agitating during the phase change. It is possible to break them down into four distinct categories.

The first strategy for an LHTES system is to incorporate ultrasonic vibrations into the system, which improves the system's performance by avoiding the formation of solid PCM layers in the subcooled liquid PCM [23,24]. The second, a double screw heat exchanger, involves conveying the PCM through a heat exchanger's continually moving helicoidally heat transfer surface during charging / discharging operations [25]. The third is the PCM flux idea, a transport tube that flows PCM across a heated surface. The fourth option is dynamic melting. This method involves recirculating liquid PCM through an external instrument during melting to control the flow and transfer of heat. Continual mixing of the PCM with motion promotes total heat transfer and improves system efficiency by decreasing charging time and encouraging forced convection.

Moreover, while keeping the high packing factor, this method precludes PCM deterioration and phase segregation [26]. Tay et al. evaluated the PCM dynamic melting process of a tube-in-tank numerically [27] and experimentally [28], catching improvements in melting time, heat transfer, and efficacy. He and Setterwall [29] studied the prospect of enhancing the PCM's heat transfer via a dynamic storage mechanism. They showed that a direct interaction between the heat transfer medium and the storage substance improved heat transfer.

Porous structures with highly conductive properties have been devised as an alternative for PCM alone. Heat transfer conduction occurs through porous foam rather than PCM in the porous/PCM composite, resulting in increased thermal diffusion rate and effective thermal conductivity [30]. It reduces the influence of natural convection for liquid PCM, which is insignificant compared to porous foam conduction [31]. Metal foams' high cost is one of the limitations of embedding them into various PCM-based energy storage systems. However, the price of metal foam has been declining over time, thus making commercial implementation feasible [32].

Liu et al. [33] used a numerical model to study the impact of metal foam on the heat transfer of latent storage in shell-and-tube structures. It is determined that metal foam improved heat transfer by over seven times. Paraffin PCM samples embedded in nickel and copper metal foams were provided by Xiao et al. [34]. The prepared materials' thermophysical characteristics were examined and estimated. It was discovered that the use of metal foams improves the effective thermal conductivity significantly. Compared to pure paraffin, the conduction of a nickel/ paraffin foam was almost thrice higher (PCM). In a numerical study, Hossain et al. [35] studied the free convection melting process of PCMs in metal foams. The upper cavity's wall was maintained at a constant high temperature, and the others were well insulated. The findings indicate that the melting rate is reduced as the metal foam's porousness increases.

The impact of utilizing foams made of copper metal on the paraffin PCM heat transfer characteristics was investigated experimentally by Zheng et al. [36]. According to the findings, the copper metal foam could shorten the melting period by 20.5 %. Sivasankaran et al. [37] studied natural convection heat transfer in a porous medium-filled cavity with no phase change. The findings suggest that increasing the porosity of the metal foam improves natural convection heat transfer. Sardari et al. [38] evaluated the influence of heat storage size on a composite metal foam-PCM system vs. a PCM alone system using a non-dimensional analysis. They demonstrated the impact of system size and the presence of porous media on melting time reduction. They stated that the melting period is shorter for the system with a lower height for the same storage capacity and power input.

The literature review shows that using a molten PCM as the working fluid is an effective approach for heat transfer enhancement for fast charging thermal energy storage. The present study aims to investigate the thermal charging of an LHTES unit filled with a metal foam and enhanced with a mixed convection flow of liquid nano-enhanced PCM for the first time. The impact of foam porosity, inlet pressure of liquid nano-enhanced PCM, and HTF inlet fluid velocity on the charging behavior of the LHTES are addressed.

2. Model description and formulation

2.1. Model description

Fig. 1(a) shows the thermodynamic cycle of dynamic charging. Here two cycles are involved with the charging (melting process) and one cycle for the discharging (solidification). A heat transfer fluid (HTF) is able to flow inside the tube and completes the heating and cooling cycles. A nano-enhanced PCM (NePCM) cycle also re-heats and circulates the NePCM inside the shell. The HTF cycle keeps the NePCM cycle in a liquid state and prevents it from solidification. Fig. 1(b)-(d) illustrates a cylindrical LHTES filled with copper metal foam saturated by coconut oil. Next to the HTF tube, a liquid NePCM inlet allows a flow of molten coconut oil-CuO NePCM inside the enclosure. The HTF flow is separated from the shell side and NePCM inlet using a copper tube of thickness C. The HTF is water that passes through the central tube with a uniform inlet velocity of U_{in}. In the present design, the tube and its inside are smooth. However, using corrugated tubes and wire coils, as explained in [39,40] could be applied to improve the heat transfer.

Initially, the NePCM inside the enclosure is supper cold at an initial solid-state. A flow of HTF with uniform temperature T_h streams through the inner tube, which heats the tube wall and NePCM near the tube wall. The HTF loses some heat to the surrounding NePCM and leaves the tube at the top under a zero-gauge pressure outflow condition.

Moreover, there is a stream of liquid NePCM with a uniform pressure P_0 at the enclosure inlet. However, the solid NePCM blocks the inlet flow of liquid NePCM. After a while, the HTF flow melts a layer of NePCM next to the tube wall and opens a passage through solid NePCM, in which the hot liquid NePCM can reach the enclosure outlet at the top. The outlet is at a gauge pressure of zero. The formation of a liquid PCM film is an important key feature of this design which allows the stream of liquid PCM moves through the enclosure.

2.2. Formulation

The governing equations and the corresponding boundary conditions are extracted and presented separately according to the notation of Fig. 2. The flow fields of the water in the central tube and the NePCM in the LHTES section are within the laminar flow range. Moreover, a local thermal equilibrium is established between the copper foam and coconut-CuO PCM. In the subsequent section, the governing equations for the HTF central tube, the composite metal foam NePCM, and the solid wall of the HTF tube will be discussed.

The equations of continuity, momentum, and energy in the HTF tube presented in the cylindrical coordinate system are as follows [41–43]:

For heat transfer fluid (HTF):

$$\frac{1}{r}\frac{\partial(ru)}{\partial r}+\frac{\partial w}{\partial z}=0 \tag{1}$$

$$\rho_{HTF}\left(\frac{\partial u}{\partial t}+u\frac{\partial u}{\partial r}+w\frac{\partial u}{\partial z}\right)=-\frac{\partial p}{\partial r}+\frac{\mu_{HTF}}{r}\frac{\partial}{\partial r}\left(r\frac{\partial u}{\partial r}\right)-\frac{\mu_{HTF}u}{r^2}+\mu_{HTF}\frac{\partial^2 u}{\partial z^2} \tag{2}$$

$$\rho_{HTF}\left(\frac{\partial w}{\partial t}+u\frac{\partial w}{\partial r}+w\frac{\partial w}{\partial z}\right)=-\frac{\partial p}{\partial z}+\frac{\mu_{HTF}}{r}\frac{\partial}{\partial r}\left(r\frac{\partial w}{\partial r}\right)+\mu_{HTF}\frac{\partial^2 w}{\partial z^2} \tag{3}$$

$$(\rho C_p)_{HTF}\left(\frac{\partial T}{\partial t}+u\frac{\partial T}{\partial r}+w\frac{\partial T}{\partial z}\right)=\frac{1}{r}\frac{\partial}{\partial r}\left(k_{HTF}r\frac{\partial T}{\partial r}\right)+\frac{\partial}{\partial z}\left(k_{HTF}\frac{\partial T}{\partial z}\right) \quad (4)$$

The variables u and w of the above-expressed equations are the velocity variables along the horizontal and vertical directions. p is the pressure variable, T is the temperature variable, and t is the time. Moreover, ρ, μ, k, and C_p stands for density, dynamic viscosity, sensible heat capacity, and thermal conductivity, respectively. The subscripts HTF indicates the heat transfer fluid.

For the composite open foam and NePCM inside the pores, the equations of continuity, momentum, and energy are established. It should be noted that the continuity equation for the melted phase change material is exactly the same as Eq. (1).

$$\frac{\rho_{NePCM}}{\varepsilon}\frac{\partial u}{\partial t}+\frac{\rho_{NePCM}}{\varepsilon^2}\left(u\frac{\partial u}{\partial r}+w\frac{\partial u}{\partial z}\right)=-\frac{\partial p}{\partial r}+\frac{\mu_{NePCM}}{\varepsilon}\left(\frac{1}{r}\frac{\partial}{\partial r}\left(r\frac{\partial u}{\partial r}\right)-\frac{u}{r^2}+\frac{\partial^2 u}{\partial z^2}\right)-\frac{\mu_{NePCM}}{K}u-s(T)u \quad (5)$$

$$\frac{\rho_{NePCM}}{\varepsilon}\frac{\partial w}{\partial t}+\frac{\rho_{NePCM}}{\varepsilon^2}\left(u\frac{\partial w}{\partial r}+w\frac{\partial w}{\partial z}\right)=-\frac{\partial p}{\partial z}+\frac{\mu_{NePCM}}{\varepsilon}\left(\frac{1}{r}\frac{\partial}{\partial r}\left(r\frac{\partial w}{\partial r}\right)+\frac{\partial^2 w}{\partial z^2}\right)-\frac{\mu_{NePCM}}{K}w-s(T)w+\rho_{NePCM}g\beta_{NePCM}(T-T_f) \quad (6)$$

$$(\rho c_p)_{NePCM,eff}\frac{\partial T}{\partial t}+(\rho c_p)_{PCM,l}\left(u\frac{\partial T}{\partial r}+w\frac{\partial T}{\partial z}\right)+\varepsilon\rho_{PCM,l}L_f\frac{\partial \omega(T)}{\partial t}=k_{NePCM,eff}\left(\frac{1}{r}\frac{\partial}{\partial r}\left(\frac{\partial T}{\partial r}\right)+\frac{\partial^2 T}{\partial z^2}\right) \quad (7)$$

where s is the sink term for velocity control in solid and liquid regions, β is the volumetric thermal expansion, g is the gravity acceleration, and L_f is the latent heat of fusion. The subscript NePCM indicates the NePCM. Here, K and ε are the metal foam permeability and porosity. The foam permeability is computed using the following equation [44]:

$$K=d_p^2\frac{73\times10^{-5}}{(1-\varepsilon)^{0.224}}\left(d_l d_p^{-1}\right)^{-1.11},\left(d_l d_p^{-1}\right)=1.18\left(\frac{1-\varepsilon}{3\pi}\right)^{0.5}[1-exp(-(1-\varepsilon)/0.04)]^{-1},d_p=0.0254\Big/\gamma\,(PPI) \quad (8)$$

and $\gamma = 5$ PPI.

Here, $s(T)=A_{mush}\frac{1-2\omega(T)+\omega^2(T)}{\lambda+\omega^3(T)}$ in which:

$$\omega(T)=\begin{cases}0 & T<T_{me}-\Delta T_{me}/2\\ \dfrac{T-T_{me}}{\Delta T_{me}}+\dfrac{1}{2} & T_{me}-\Delta T_{me}/2<T<T_{me}+\Delta T_{me}/2\\ 1 & T>T_{me}+\Delta T_{me}/2\end{cases} \quad (9)$$

In the above equation. $A_{mush}=10^{-9}$ Pa.s/m^2, and $\lambda = 0.001$is introduced to avoid division by zero, $\Delta T_{me}=10$ °C. The effective thermal properties are computed as follows:

$$(\rho C_p)_{NePCM}=(1-\phi)(\rho C_p)_{\mathrm{PCM}}+\phi(\rho C_p)_{np} \quad (10a)$$

$$\rho_{NePCM}=(1-\phi)\rho_{\mathrm{PCM}}+\phi\rho_{np} \quad (10b)$$

$$\frac{k_{NePCM}}{k_{PCM}}=\frac{k_{np}+2k_{PCM}-2\phi(k_{PCM}-k_{np})}{k_{np}+2k_{PCM}+\phi(k_{PCM}-k_{np})} \quad (10c)$$

$$\frac{\mu_{NePCM}}{\mu_{PCM}}=\frac{1}{(1-\phi)^{2.5}} \quad (10d)$$

where subscript np represents nanoparticles and ϕ is the volume fraction of nanoparticles. In the above equations, inserting the thermophysical properties of solid PCM or liquid PCM gives the effective thermophysical properties of solid and liquid NePCM, respectively. Moreover, the ultimate thermophysical properties of NePCM depend on the melting volume fraction and a weighted average of the solid and liquid NePCM with the local liquid volume fraction $\omega(T)$ as a weight. For example, the thermal conductivity of NePCM was computed as: $k_{\mathrm{NePCM}} = \omega \times k_{\mathrm{NePCM,l}} + (1\text{-}\omega)\, k_{\mathrm{NePCM,s}}$. Ultimately, the effective thermophysical properties of composite NePCM and metal foam were computed as a weighted average of NePCM and the metal foam as:

$$\chi_{eff,NePCM}=\varepsilon\chi_{NePCM}+(1-\varepsilon)\chi_{foam}$$

$$\chi_{eff}=\varepsilon\chi_{NePCM}+(1-\varepsilon)\chi_{foam} \quad (11)$$

where χ_{eff} stands for any effective thermophysical properties such as thermal conductivity (k), density (ρ), or heat capacity (ρC_p). The energy conservation equation for copper tube as a solid intermediate thick wall is computed as:

$$(\rho c_p)_w\frac{\partial T}{\partial t}=k_w\left(\frac{1}{r}\frac{\partial}{\partial r}\left(\frac{\partial T}{\partial r}\right)+\frac{\partial^2 T}{\partial z^2}\right) \quad (12)$$

where subscript w indicates the thick wall.

2.3. Controlling boundary and initial conditions

The HTF is injected with the temperature of T_h, and velocity of U_{in}.

$$T_{HTF}=T_h,u_{HTF}=0,\quad w_{HTF}=U_{in} \quad (13)$$

At the outlet of the HTF tube, the developed convective flow is considered to be established.

$$u_{HTF}=0,P_{HTF}=0,\left.\frac{\partial T}{\partial z}\right|_{HTF}=0 \quad (14)$$

The injected NePCM in the bottom to up direction can be written as:

$$P_{NePCM}=P_{in}\quad and\quad \mathrm{T}_{NePCM}=T_h \quad (15a)$$

And at the outlet, it is expected:

$$u_{NePCM}=0,P_{NePCM}=0,and\left.\frac{\partial T}{\partial z}\right|_{NePCM}=0 \quad (15b)$$

The perimeter wall of the enclosure is well insulated, and hence, the boundary conditions at the outer wall are:

$$u_{NePCM}=w_{NePCM}=0,\left.\frac{\partial T}{\partial r}\right|_{NePCM}=0 \quad (16)$$

At the upper and lower surfaces of the NePCM enclosure, the boundary conditions are defined as the following:

$$u_{NePCM}=w_{NePCM}=0,\left.\frac{\partial T}{\partial z}\right|_{NePCM}=0 \quad (17)$$

The continuity of temperature and heat flux at the inner and outer tube walls was considered between the tube wall and HTF and tube wall and NePCM.

The initial condition for the PCM domain can be expressed as the following:

$$u_{NePCM}=w_{NePCM}=0,P_{NePCM}=0,T_{NePCM}=T_{initial} \quad (18)$$

2.4. Total energy stored in the unit (ES) and melting volume fraction (MVF)

The amount of energy stored, $ES(t)$, in the LHTES unit during the melting process is equal to the heat transferred from the central tube to the summation of sensible and latent heat, which can be computed as:

$$ES(t) = \overbrace{\int_V \left(\int_{T_{initial}}^{T} \left[(\rho C_p)_{eff,NePCM} + (\rho C_p)_w \right] dT \right) dV}^{Sensible\ heat} + \overbrace{\int_V \omega \rho_{NePCM,l} L_f dV}^{Latent\ heat} \quad (19)$$

Besides, the melting fraction of the phase change material at different times can be estimated through the following equation:

$$MVF(t) = \frac{\int_V \omega(T) dV}{\int_V dV} \quad (20)$$

The thermophysical properties of the materials employed in the present study include coconut oil as a phase change material in the energy storage unit, water through the HTF central tube, copper plate between the water and the phase change material, and copper foam, which are listed in Table 1.

Furthermore, the velocity of the heat transfer fluid (HTF) at the inlet of the mentioned tube is equal to 0.1 m/s, and the inlet pressure of the storage unit is considered 3000 Pa. The inlet temperature of the storage unit and HTF tube is equally set to 60 °C. The LHTES unit is at an initial temperature of 15 °C, which is well below the fusion temperature, and NePCM is super cold.

3. Numerical method and validation

3.1. Finite element method (FEM)

The FEM, founded on a weighted residual method, is applied to integrate the model's equations. The partial differential equations controlling the conservation of mass, momentum, and energy were transformed into a weak form and then integrated over mesh elements or obtain the residual equation. Then, the residual equations were solved iteratively for field variables. Fig. 2 depicts the flow chart of solution steps. The Newton method was employed to solve the equations in a fully coupled form. The backward differential formula with the PARDISO solver was invoked to control the time steps and keep the accuracy of the solutions with a relative error of 10^{-4}. The computations were continued until the MVF reached 0.999, indicating a fully melted enclosure.

3.2. Mesh study

The influence of the adopted mesh sizes on the accuracy of the solutions was examined in this section. For this purpose, the melting fraction, the amount of stored energy, and the average velocity of the liquid NePCM at the LHTES's outlet were monitored for four different mesh sizes in the period of 0 to 8000 s. The results are illustrated in Fig. 3 for $\varepsilon = 0.8$, $P_{in} = 3000$ Pa, $VF_{na} = 0$, $T_h = 50$ °C, and $U_{in} = 0.1$ m/s. The details of the mesh sizes for four cases I-IV are listed in Table 2. A nonuniform mesh with a stretching ratio of 1/20 was applied to the HTF region to capture the boundary layer flow and temperature gradients adequately.

As it turns out, all four cases are very close to each other over the entire period. However, it is important to note that for a coarse mesh, the efficiency of the solver to capture the melting interface declines adequately, and some convergence issues arise. However, the computational costs also increase drastically for a very fine mesh. Therefore, the third case was selected as the computational mesh for a cost-efficient and converged solution. All the results of this study were computed based on this mesh size. Fig. 4 depicts a view of the selected mesh for Case 3.

3.3. Validation of the numerical method

The simulation results were verified through comparison with the experimental data reported by Kamkari et al. [47], where the stored energy in a rectangular LHTES unit during the melting of a PCM is plotted in Fig. 5. Besides, the melting of paraffin wax embedded in open-cell copper foam was simulated, and a good match was observed with experimental data [36]. More details can be found in [48].

4. Results and discussion

In the first step, the impact of HTF velocity inlet, NePCM pressure inlet, and foam porosity on the thermal behavior of the LHTES unit was addressed while the volume fractions of nanoparticles were zero. Secondly, the effect of nanoparticles on the unit's heat transfer was investigated. Table 3 depicts the investigated parameters and their values. The simulation results are displayed in the form of melting fraction (*MVF*), stored energy, isotherms, and streamlines. Table 4 summarizes the combination of the control parameters for each investigated case.

Figs. 6 (a) to (d) exhibit the effect of the porosity ε on the melting fraction, the amount of stored energy, the discharge rate from the unit, and the average temperature of the liquid PCM leaving the unit. The study was performed for four values of the porosity in the high range $\varepsilon =$ 0.85, 0.9, 0.95 *and* 0.975. As seen in Fig. 6(a), all four curves change abruptly over a particular period, and then the melting process is completed sharply. In this design, the initial melting is very important. It should be noted that the solid PCM blocks the flow of liquid PCM at the inlet. Thus, as soon as a layer of liquid PCM forms around the HTF tube inside the enclosure, the blockages weaken, and a forced convection stream of molten PCM would be possible. A composite PCM with a low porosity provides a better composite thermal conductivity since there will be more solid foam. However, a higher effective thermal conductivity would pass the absorbed heat from the tube to a wider region of solid PCM and delay the initiation of the first liquid layer around the HTF tube. Thus, as seen in Fig. 6(a), there is a critical inversion point in which a higher MVE could be observed for $\varepsilon = 0.85$ than $\varepsilon = 0.9$, but for $\varepsilon = 0.95$ and $\varepsilon = 0.975$, it becomes higher than a porosity of 0.85.

For the case of foam with low porosity, permeability is another significant parameter that contributes to mixed convection heat transfer. A foam with low porosity imposes a significant flow resistance (low permeability) on the liquid stream and limits the forced convection flow. However, the low porosity also means a better overall effective thermal conductivity, accelerating thermal energy storage. Thus, as seen, a foam with $\varepsilon = 0.85$ could better charge the LHTES unit compared to that of $\varepsilon = 0.9$.

Fig. 6(c) shows that the output flow rate increases as the porosity increases due to the decrease in permeability. According to Fig. 6(d), in the initial times, the temperature of the PCM in the area adjacent to the heated tube rises with a gentle slope. When a liquid film forms, the liquid PCM starts to flow, and a steep slope occurs. The outlet temperature increases since a heated flow of liquid PCM also enters the unit. It is important to note that the outlet temperature at the end of the charging process is fixed at about 330 ± 3 K, and it does not change much with the foam's porosity. According to the considered thermal boundary conditions at the unit's inlet (inlet temperature 333 K), it can be understood that after the completion of the melting process, the liquid PCM reaches the outlet with a minimum temperature drop.

Figs. 7 and 8 show the isotherms and streamlines for the lower and

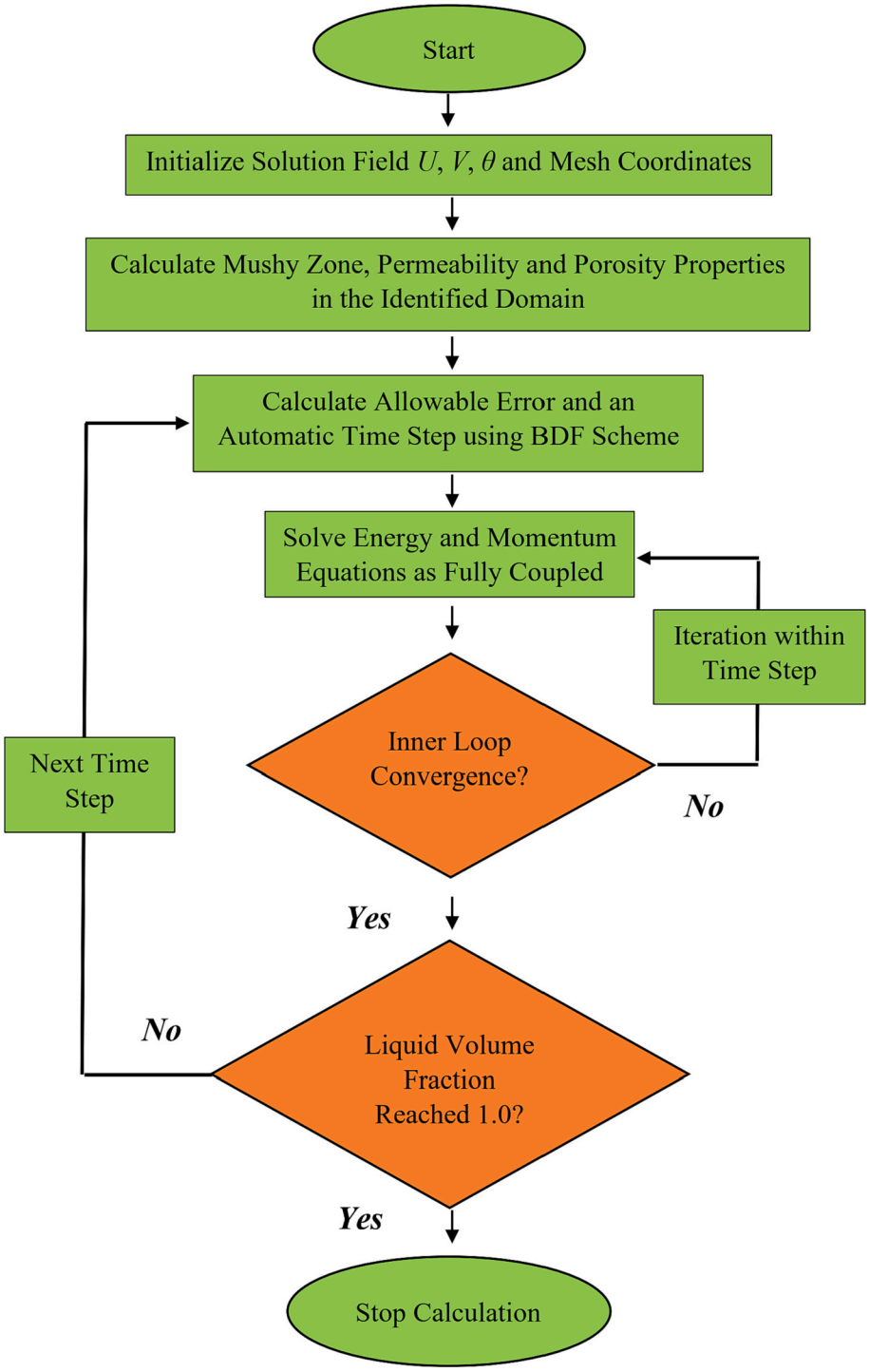

Fig. 2. The flowchart of the computational algorithm and computational steps.

Table 1
Thermophysical properties of Coconut oil and the nano-additives [45,46].

Properties	Coconut oil (measured)		HTF (water at T_{in})	Copper tube and foam
	Solid (15 °C)	Liquid (32 °C)		
ρ_{PCM} (kg m^{-3})	920	914 ± 0.11 %	993.73	8900
μ_{PCM} (Nsm^{-2})	–	0.0326 ± 3 %	0.705 × 10^{-3}	–
C_p (J kg K^{-1})	3750	2010 ± 0.2 %	4178	386
k (W m^{-1} K^{-1})	0.228	0.166 ± 1.2 %	0.623	380
h_f (kJ kg^{-1})		103 ± 1 %		–
Pr		394.73 ± 3.2 %		–
T_{me} (ΔT_{me})	24 °C (±1 °C)			–

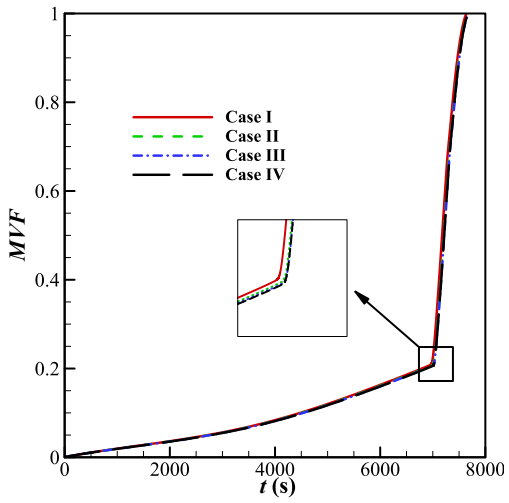

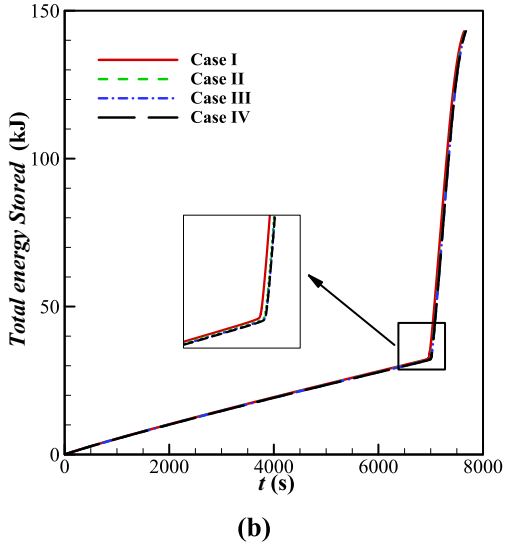

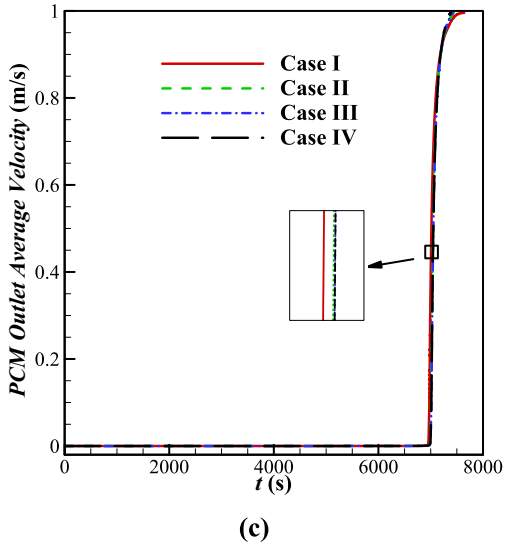

Fig. 3. Mesh independency of the results on mesh size for; (a) Melting volume fraction, (b) Total energy stored, and (c) NePCM outlet average velocity.

higher considered values of the porosity, i.e., 0.85 and 0.975, at three time-snaps of 1000 s, 5500 s, and 11,000 s. As can be seen, the melting front quickly develops in the enclosure when the porosity is high. In this case, the temperature gradients were mainly shifted to the top right corner of the enclosure, where there is a weak convection circulation. Contrarily, the melting front develops in the enclosure with a significant delay compared to the case of high porosity.

Fig. 8 shows a natural convective circulation inside the enclosure at initial times when there is no significant forced convection flow. As soon as the solid PCM is melted, the stream of inlet liquid PCM follows from

Table 2
The specification of utilized structured mesh in the enclosure.

Mesh case	Horizontal intervals					Vertical interval
	Total NEPCM	Inlet/ outlet	Rest of NEPCM	Wall	HTF tube	
I	40	10	30	2	10	50
II	60	15	45	3	15	75
III	80	20	60	4	20	100
IV	100	25	75	5	25	125

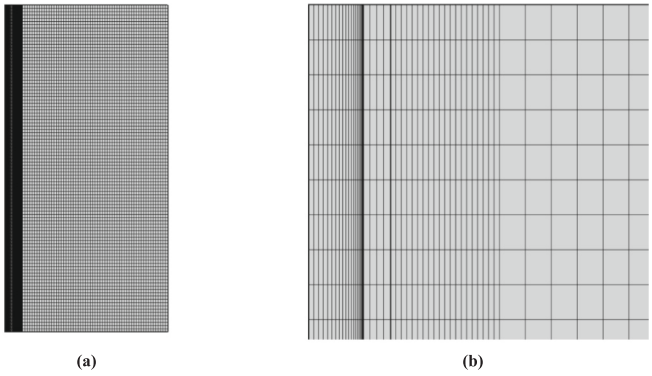

Fig. 4. Views of the chosen grid mesh; (a) Overall geometry, and (b) Focused on the left top corner.

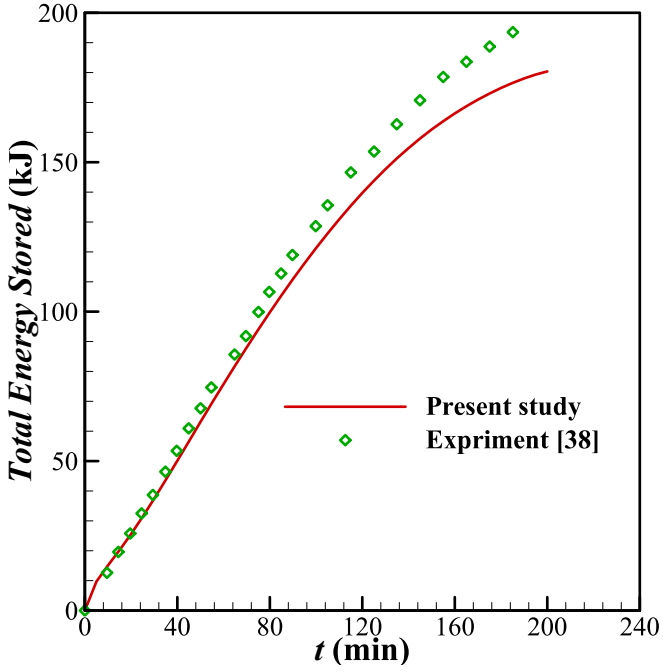

Fig. 5. The stored energy simulated in the present study and those measured in [47].

Table 3
The name and magnitude of the investigated parameters.

Factors	Description	Level 1	Level 2	Level 3	Level 4
A	ε Porosity	0.85	0.90	0.95	0.975
B	P_{in} Pressure inlet [Pa]	1000	2000	3000	4000
C	U_{in} HTF velocity inlet [m/s]	0.05	0.075	0.1	0.125

Table 4
Details of investigated cases and the thermal charging time.

Case	Parameter	A	B	C	Full melting
		ε	P_{in} (Pa)	U_{in} (m/s)	Time (s)
1	ε	0.85	3000	0.1	13,829
2		0.90	3000	0.1	14,976
3		0.95	3000	0.1	7640
4		0.975	3000	0.1	2492
5	P_{in}	0.95	1000	0.1	8604
6		0.95	2000	0.1	7954
7		0.95	3000	0.1	7639
8		0.95	4000	0.1	7428
9	U_{in}	0.95	3000	0.05	16,070
10		0.95	3000	0.075	11,222
11		0.95	3000	0.1	8605
12		0.95	3000	0.125	7038

the inlet toward the outlet. After melting a substantial amount of PCM, a uniform streamlines distribution can be observed in the middle of the enclosure. Over time, as the melting front progresses, the width of the streamlines inside the enclosure grows, and the size of the melted PCM region develops. For the lowest porosity, i.e., $\varepsilon = 0.85$, the outlet is not fully open yet, and hence the melting is slow and is mainly controlled by the conduction and natural convection circulation mechanisms. These outcomes are in good agreement with the results of Fig. 6(a) and (c).

As described in the schematic diagram for the boundary conditions, the high-temperature, pressurized liquid PCM enters the unit when there is a feasible passage between the inlet and outlet. As shown in Figs. 9, an increase in the static pressure at the inlet of the enclosure considerably improves the MVF, the total stored energy, the flow rate, and the average outlet temperature. Keeping the foam's porosity at a constant value takes less time for the high-pressure melted PCM to open a passage through the melted PCM and extend the passage. As a passage develops between the inlet and the outlet, a constant stream of heated liquid PCM can enter the enclosure. The forced convective melting of the PCM inside the enclosure would be feasible. In fact, when the PCM enters the enclosure with high pressure, the exit path opens much faster, the hot PCM enters the chamber at a higher pace, and in general, the LHTES unit would be charged in a shorter period of time. It should be noted that raising the static pressure at the enclosure's inlet accelerates the charging time and does not enhance the charge level.

The outlet flow through the chamber elevates as a function of the high-pressure phase change material (Fig. 9(c)). However, raising or reducing the pressure as a flow parameter does not change the temperature patterns (Fig. 9(d)). Indirectly, the increase in pressure leads to a growth in the outlet flow rate of the chamber, and as mentioned

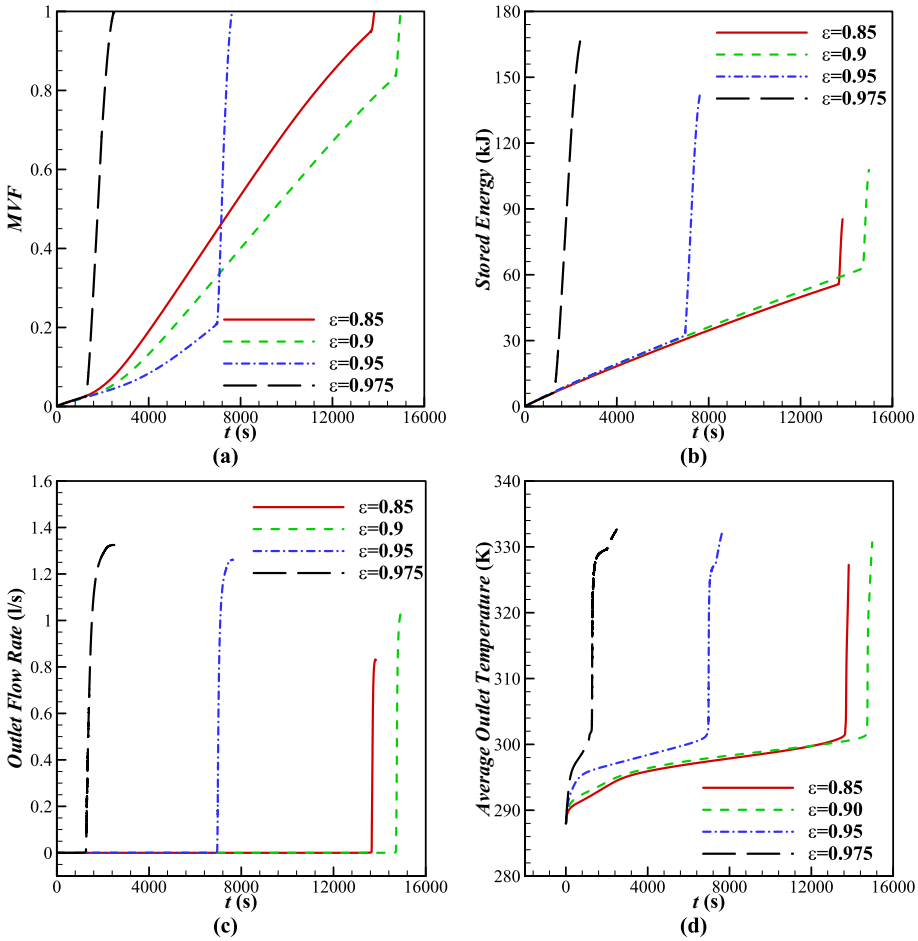

Fig. 6. Effect of porosity parameter (ε) on; (a) Melting volume fraction, (b) Total energy stored, (c) Outlet flow rate, and (d) Average outlet temperature.

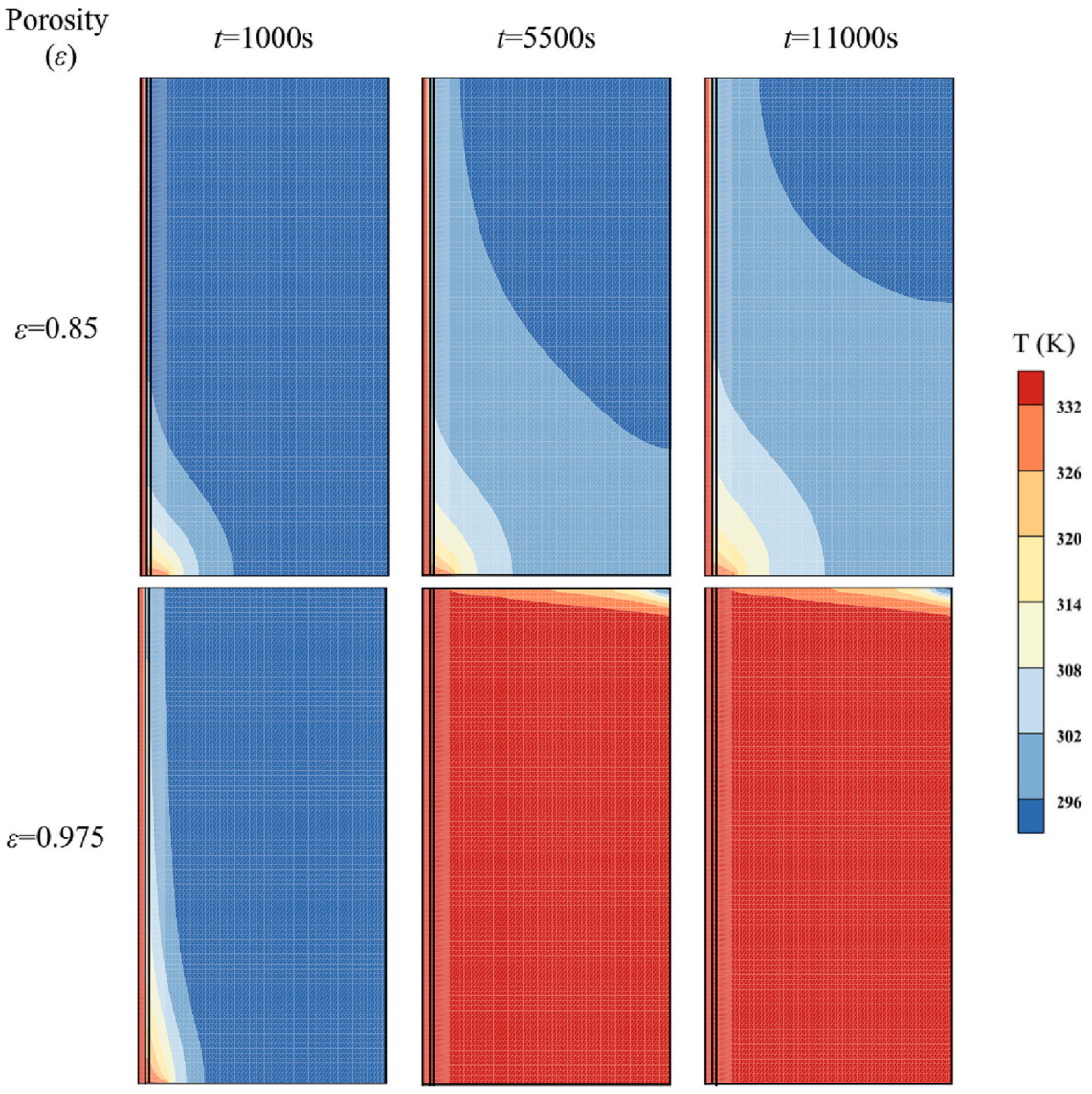

Fig. 7. Effect of porosity parameter on the contours of isotherm; (Top row) Case 1 with $\varepsilon = 0.85$, and (Bottom row) Case 4 with $\varepsilon = 0.975$, in the three different times.

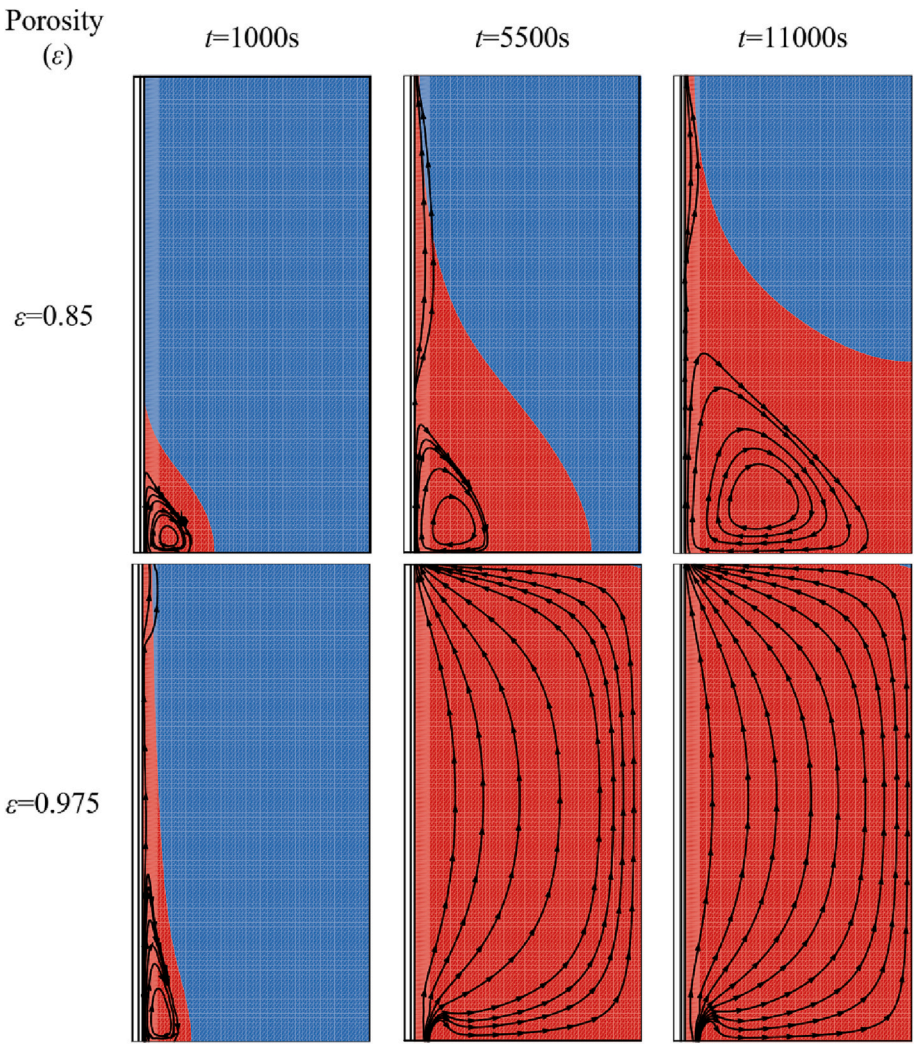

Fig. 8. Effect of porosity parameter on the streamlines; (Top row) Case 1 with $\varepsilon = 0.85$, and (Bottom row) Case 4 with $\varepsilon = 0.975$, in the three different times.

earlier, the increase in the flow rate only causes the molten fluid to reach the maximum temperature faster; but, all four curves have reached the temperatures above 330 K at the end of melting.

The effect of the inlet pressure on the isotherms and streamlines in three time-snaps of 1000 s, 5500 s, and 11,000 s is illustrated in Figs. 10 and 11. Based on the obtained results, the width of the constant isotherms in primary and secondary times are very similar. In contrast, in the last time instance and for higher inlet pressure, the mentioned lines in the upper right corner of the enclosure are more compact than for the low inlet pressure. Therefore, a slight temperature gradient occurs throughout the chamber, and the chamber homogenously remains at a temperature above 330 K.

As it turns out, here, both the melting front pattern and the flow lines are similar for the minimum and maximum inlet pressures in the first and second times. The final stage of the melting process occurs at about 11,000 s when the melting process of the PCM is completed. A closer look at the streamlines reveals that the streamline patterns which ultimately developed in the enclosure are different for the minimum and maximum inlet pressures. The streamlines distributions are uniform and inclined to the right wall for the lowest and highest inlet pressures. Additionally, the high inlet pressure causes the generation of a cluster-like structure in the streamlines at the inlet and outlet of the enclosure since the inlet flow rate grows.

Contours in Fig. 12 exhibit the effect of HTF inlet velocity entering the tube on the *MVF*, the total stored energy, the LHTES outlet flow rate, and the average temperature of the liquid PCM leaving the enclosure. As shown in Fig. 12(a), elevating the inlet velocity increases the melting fraction of the PCM and, consequently, raises the stored energy. As the inlet HTF velocity increases, the dimensionless Reynolds number for the minimum and maximum velocities reaches 895 and 2238, respectively, which is still in the laminar flow.

By rising the inlet velocity of the HTF, heat transfer from the thick tube to the PCM is enhanced. The initial film is then formed quickly inside the PCM storage unit and boosts the development of forced convection inside the enclosure. Hence, the melting process and then the thermal storage ultimately completes faster. Thus, the formation of liquid film is the key to the fast-charging process.

The effect of the inlet flow velocity on isotherms and streamlines at three time-snaps of 1000 s, 5500 s, and 11,000 s is shown in Figs. 13 and 14. Based on these time-snaps, the difference between the resulting patterns of 1000s and 5500 s is negligible. However, for the time-snap $t = 11{,}000$ s, the unit with an HTF inlet velocity of 0.125 m/s has reached the fully melted state, while the unit with an inlet velocity of 0.05 m/s has not reached the steep state and did not benefit from the forced convection heat transfer provided by liquid PCM.

Fig. 14 shows that the progress of the melting front is completely in agreement with the isotherms. For both cases of HTF inlet velocities of 0.125 m/s and 0.05 m/s, the streamlines are very similar at the initial time-snaps of 1000s, where the liquid PCM film has not reached the outlet yet. For case, $U_{\underline{in}} = 0.125$ m/s, the liquid film has reached the

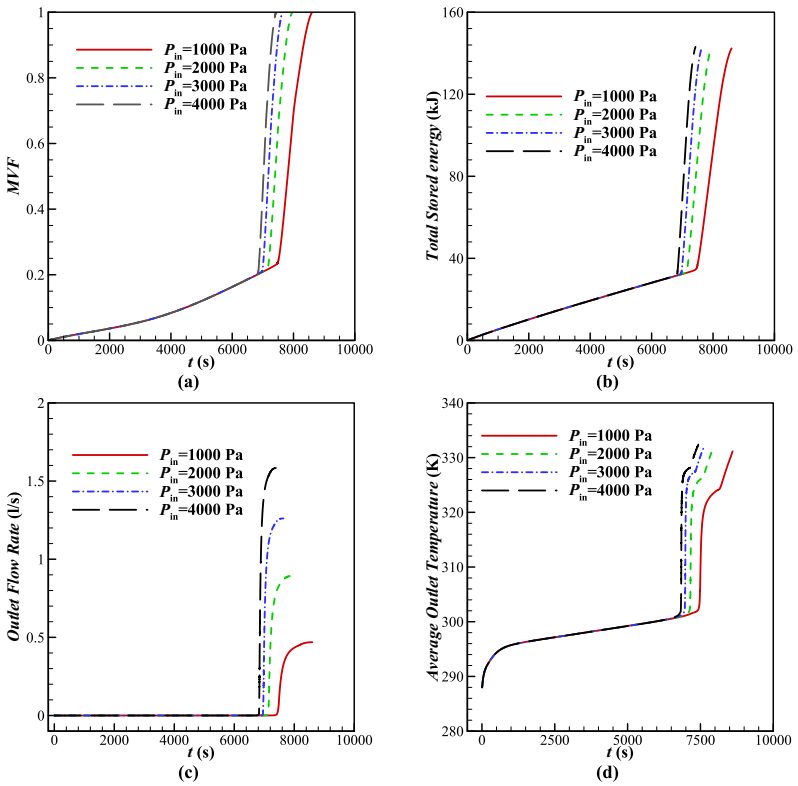

Fig. 9. Effect of inlet pressure (P_{in}) on; (a) Melting volume fraction, (b) Total stored energy, (c) Outlet flow temperature, and (d) Average outlet temperature.

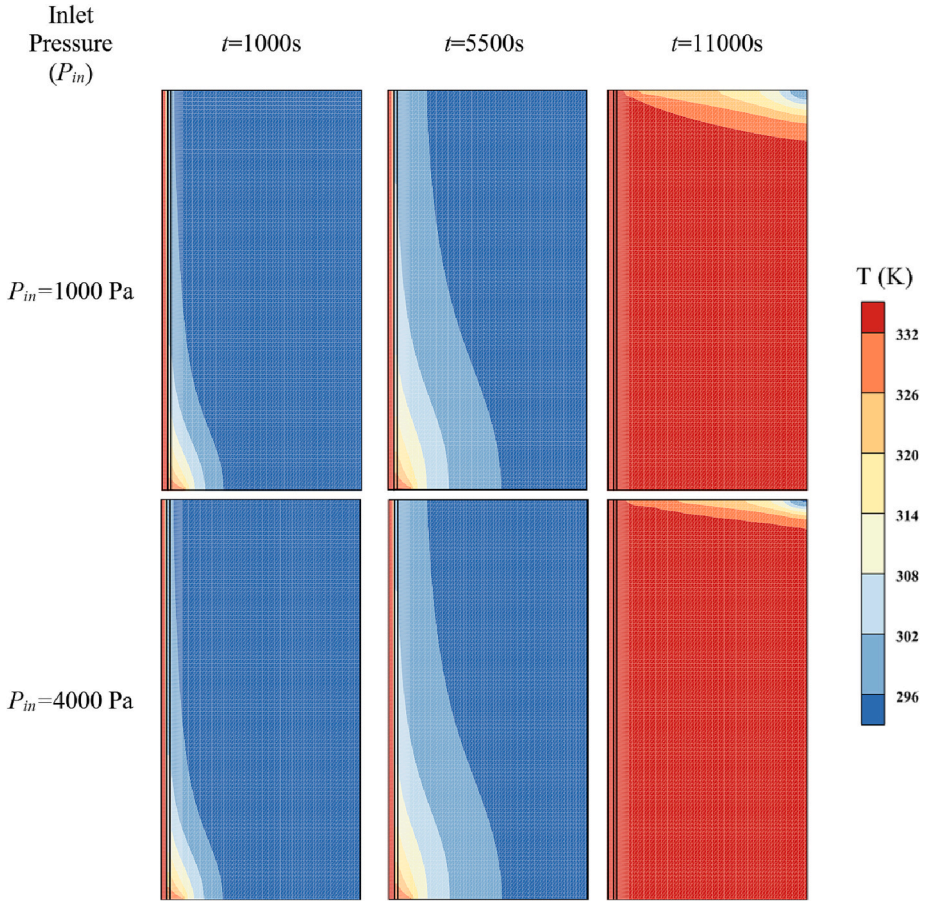

Fig. 10. Effect of inlet pressure on the contours of isotherm; (Top row) Case 5 with P_{in} = 1000 Pa, and (Bottom row) Case 8 with P_{in} = 4000 Pa, in the three different times.

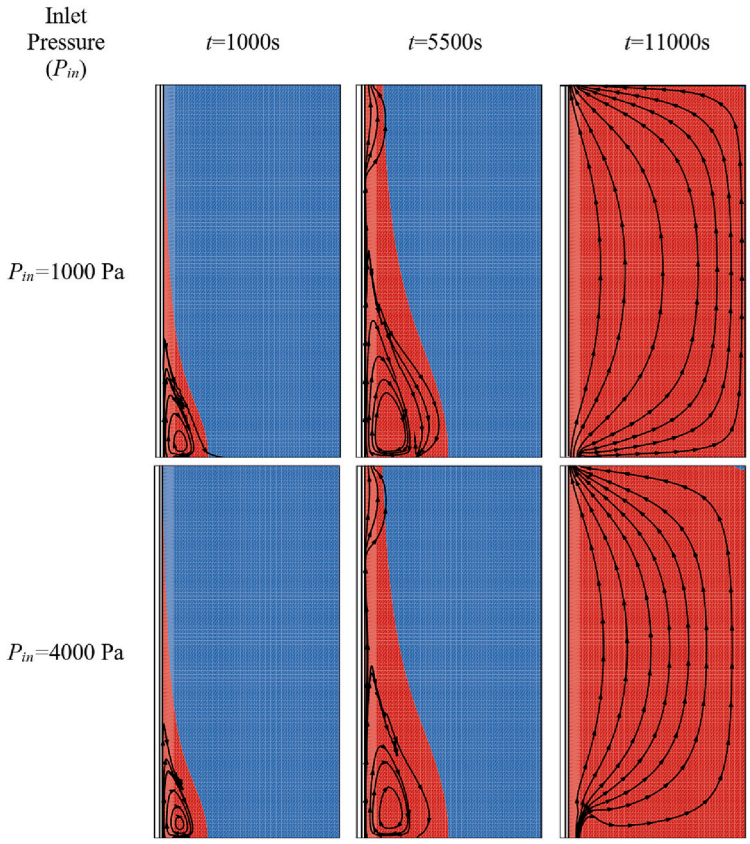

Fig. 11. Effect of inlet pressure on the streamlines; (Top row) Case 5 with P_{in} = 1000 Pa, and (Bottom row) Case 8 with P_{in} = 4000 Pa, in the three different times.

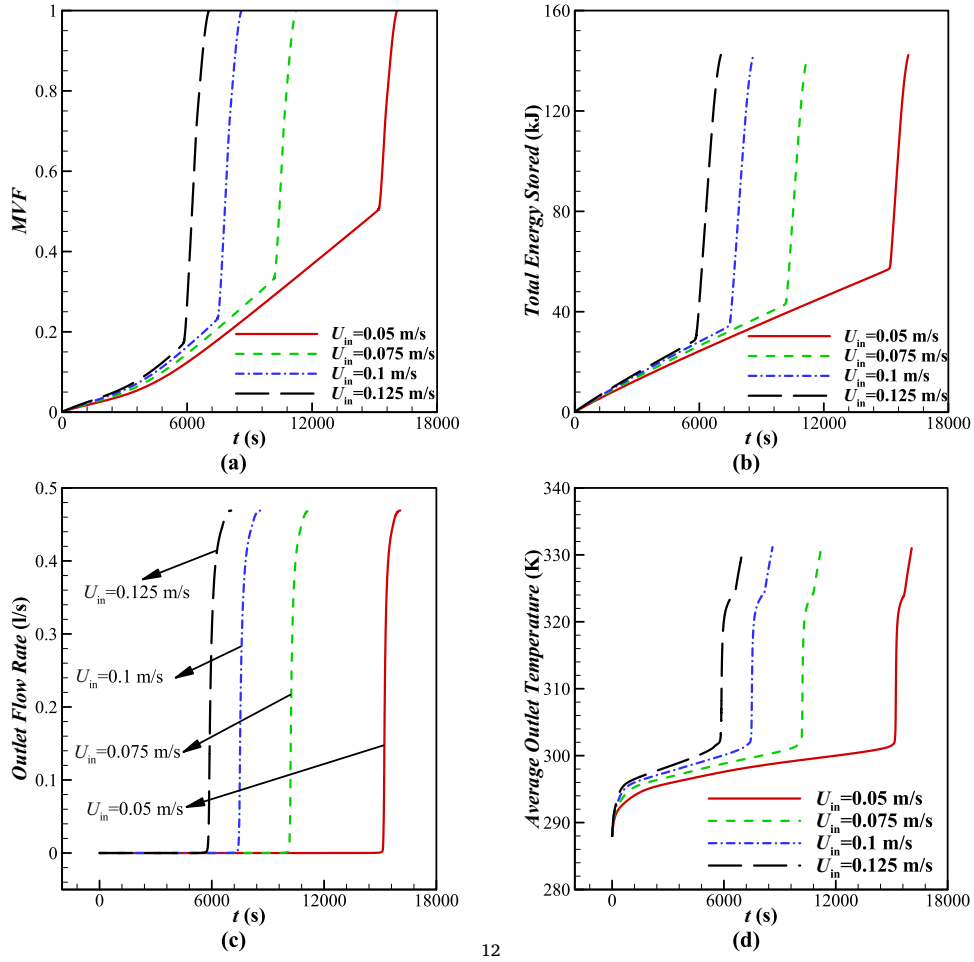

Fig. 12. Effect of inlet velocity (U_{in}) on; (a) Melting volume fraction, (b) Total stored energy, (c) Outlet flow rate, and (d) Average outlet temperature.

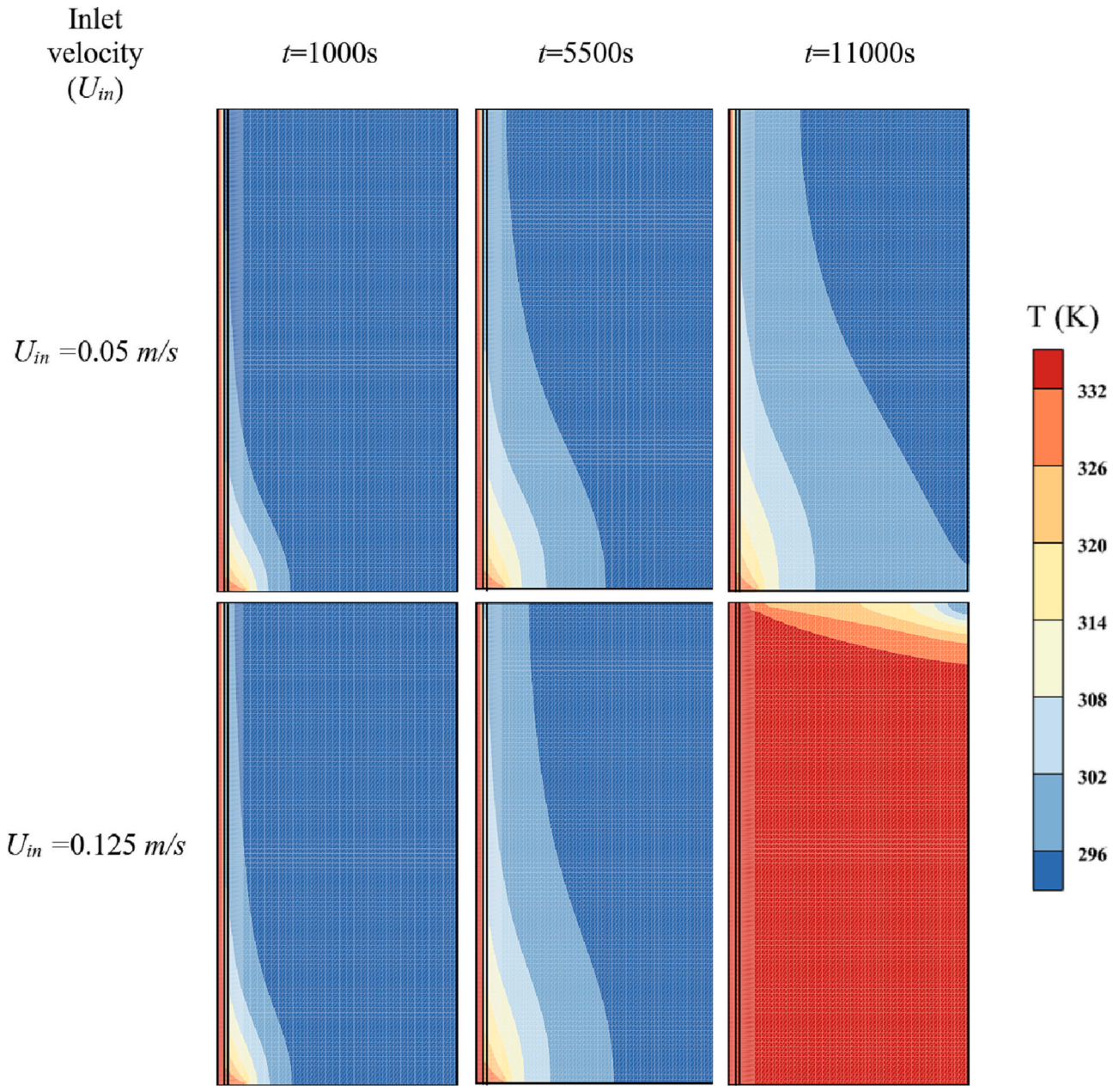

Fig. 13. Effect of inlet velocity on the contours of isotherm; (Top row) Case 9 with U_{in} = 0.05 m/s, and (Bottom row) Case 12 with U_{in} = 0.125 m/s, in the three different times.

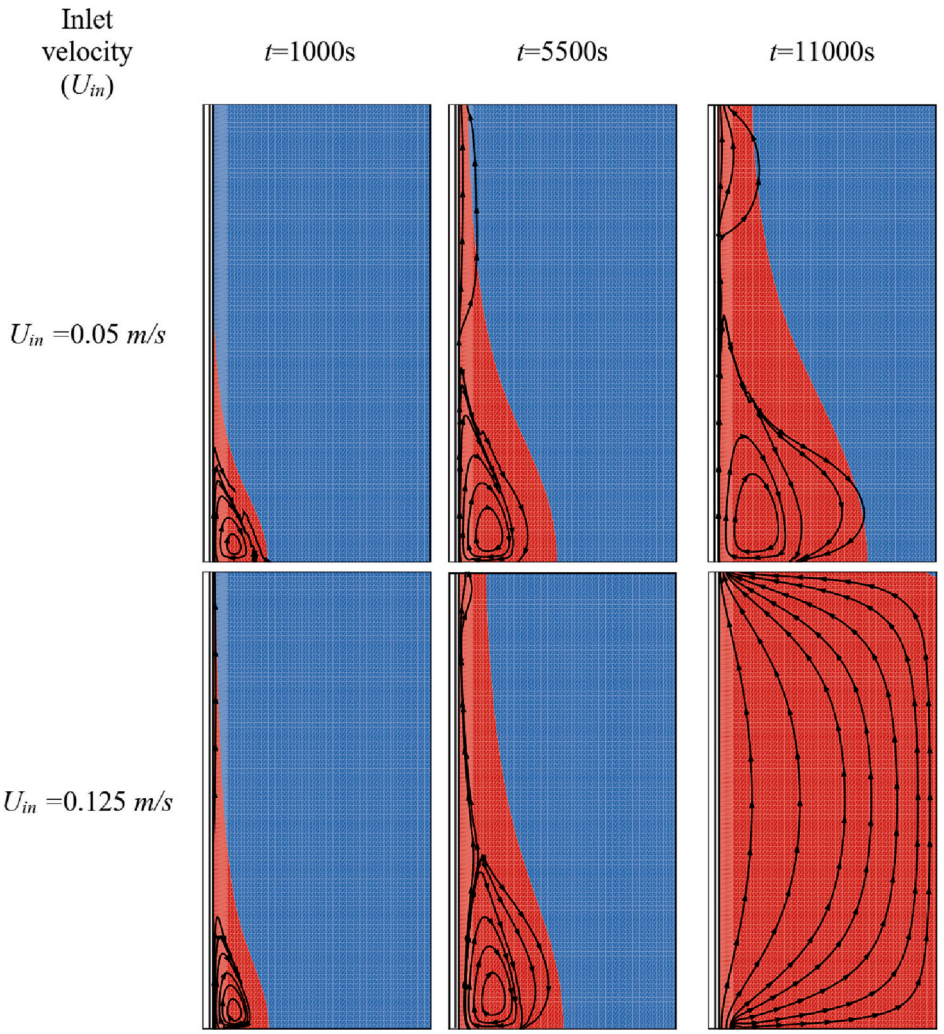

Fig. 14. Effect of inlet HTF velocity on the streamlines; (Top row) Case 9 with U_{in} = 0.05 m/s, and (Bottom row) Case 12 with U_{in} = 0.125 m/s, in the three different times.

outlet, and mixed convection consists of local natural convection at the bottom, and a smooth flow of liquid PCM from bottom to top can be observed. Time-snaps t = 11,000 s show that the unit with U_{in} = 0.125 m/s reached a fully melted state, and a uniform streamline is established inside the metal foam, while the forced convection regime is just started in the case U_{in} = 0.05 m/s.

4.1. Effect of volume fraction of the nanoparticles

In this section, the impact of the volume fraction of nanoparticles on the heat transfer behavior of the LHTES unit is investigated. Here the design variables are fixed at: ε = 0.975, P_{in} = 1000 Pa, and U_{in} = 0.075 m/s. The impact of variation of the volume fraction of nanoparticles ϕ on the MVF, total stored energy, outlet flow rate, and average outlet temperature is addressed in Figs. 15. It can be shown that the augmentation of the volume fractions of the nanoparticles reduces the MVF and the total stored energy. This is because the presence of nanoparticles improves the composite thermal conductivity and delays the formation of the initial film of liquid NePCM. The reduction in the total stored energy is also because the nanoparticles do not contribute to the latent heat energy storage and hence the overall heat capacity of a NePCM is lower than a pure PCM.

Interestingly, the presence of nanoparticles declines the outlet flow rate of liquid NePCM since the addition of nanoparticles to a liquid raises the dynamic viscosity of the mixture. The higher the dynamic viscosity, the higher the friction resistance in the metal foam, and the lower the outlet flow rate when the inlet pressure is fixed. Finally, the outlet temperature reaches the inlet boundary condition after full charging. However, since the full charging of the LHTES unit is slow by using nanoparticles, reaching the outlet temperature to the steady temperature T_h = 333 K is also done with some delays.

Figs. 16 and 17 depict the isotherms and streamlines for cases of PCM and NePCM (5 % nanoparticles volume fraction). The isotherms for the initial time t = 1000s are almost the same. As time advances, a notable difference between isotherms of PCM and NePCM can be observed at t = 2500 s. In the case of PCM, a strong liquid film is developed over the HTF tube, and the streamlines are fully connected between the liquid PCM at the inlet and the enclosure outlet. The streamlines indicate a forced convection dominant behavior inside the enclosure. For the case of NePCM, the liquid film over the HTF tube is weak, and there is a negligible forced convection flow; then, natural convection dominates the streamlines behavior inside the enclosure.

At step 4000 s, the enclosure containing PCM is in a fully melted state, while a large area of the enclosure filled with NePCM is still in a solid state. Therefore, due to the importance of developing a liquid film over the HTF tube, nanoparticles are not beneficial. Although the nanoparticles could enhance the thermophysical properties of the pure PCM, they also delay the liquid film formation, reduce the overall flow rate in the enclosure, and deteriorate the heat transfer.

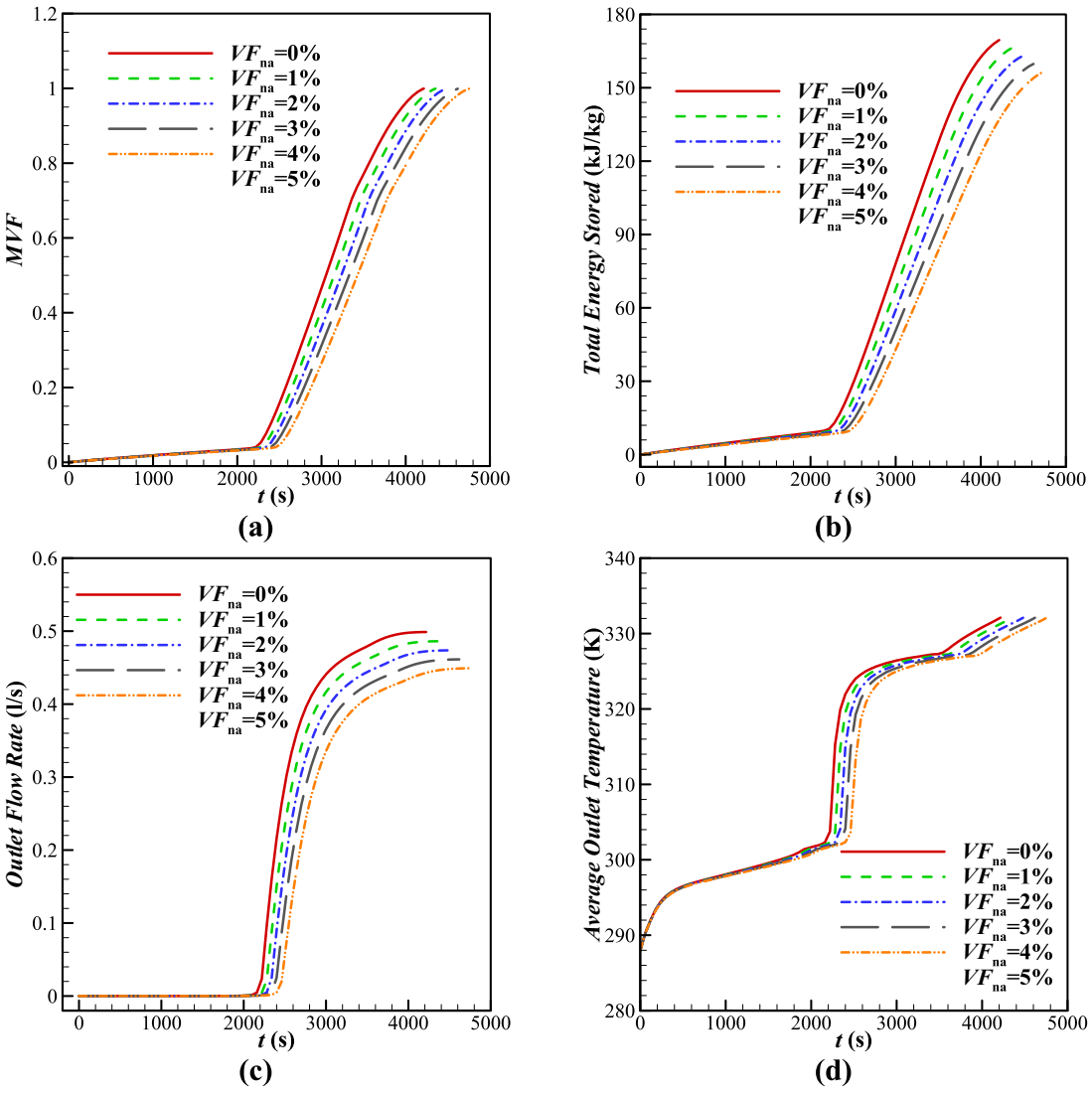

Fig. 15. Effect of volume fraction of the nanoparticles on; (a) Melting volume fraction, (b) Total stored energy, (c) Outlet flow rate, and (d) Average outlet temperature, from zero to 5000 s.

5. Conclusion

The performance of thermal energy storage with a flow of hot liquid PCM inside an LHTES unit was theoretically investigated using the FEM. A hot pressurized liquid PCM entered the storage unit from below and left the enclosure from the top. The charging behavior of the unit was strongly dependent on the formation of a liquid PCM film which allows the stream of liquid PCM from the inlet of the enclosure to its outlet. The most important results are as follows:

1. The fast-charging process is mainly dominated by the initial formation of a liquid film over HTF tube. Generally, increasing the metal foam's porosity could help the thermal charging of the enclosure by accelerating the formation of liquid film over the HTF tube. This was an unexpected result since a foam with a high porosity creates more void spaces and small composite thermal conductivity improvement. This small effective thermal conductivity was beneficial in initial liquid formation. However, for a low porosity of 0.85 and 0.9, the permeability of the foam is also important and could change the fully melting time of LHTES by limiting the liquid PCM flow rate in the enclosure. Moreover, the increase of porosity always improves the total stored energy and outlet flow liquid PCM rate since the higher the porosity, the more void space, better latent heat capacity, and higher permeability.

2. An increase in the inlet pressure at the enclosure inlet reduces the charging time and increases the outlet flow rate and the average temperature. However, increasing the inlet pressure is only beneficial when there is a passage between the enclosure's inlet and outlet.

3. An increase in the HTF inlet velocity could significantly reduce the charging time of the LHTES. It also reduces the required time needed to reach the maximum flow rate and the average outlet temperature. Indeed, the HTF inlet velocity could accelerate the film formation of liquid PCM over the HTF tube in the PCM enclosure. Consequently, the forced convection heat transfer due to the stream of hot PCM liquid occurs sooner, and the charging time of the unit declines notably. By raising the HTF inlet velocity by 2.5 times from 0.05 m/s to 0.125 m/s, the required time for a full charge of the unit decreases at the same rate.

4. Using nano-additives enhances thermal conductivity; however, the presence of nanoparticles delays the formation of liquid film over the HTF tube and slows down the overall charging time of the unit. Moreover, nano-additives do not contribute to latent heat energy storage and decline the unit's overall thermal energy storage capacity. Thus, in this particular design of fast thermal charging LHTES unit, using nano-additives is not beneficial and could deteriorate the melting process.

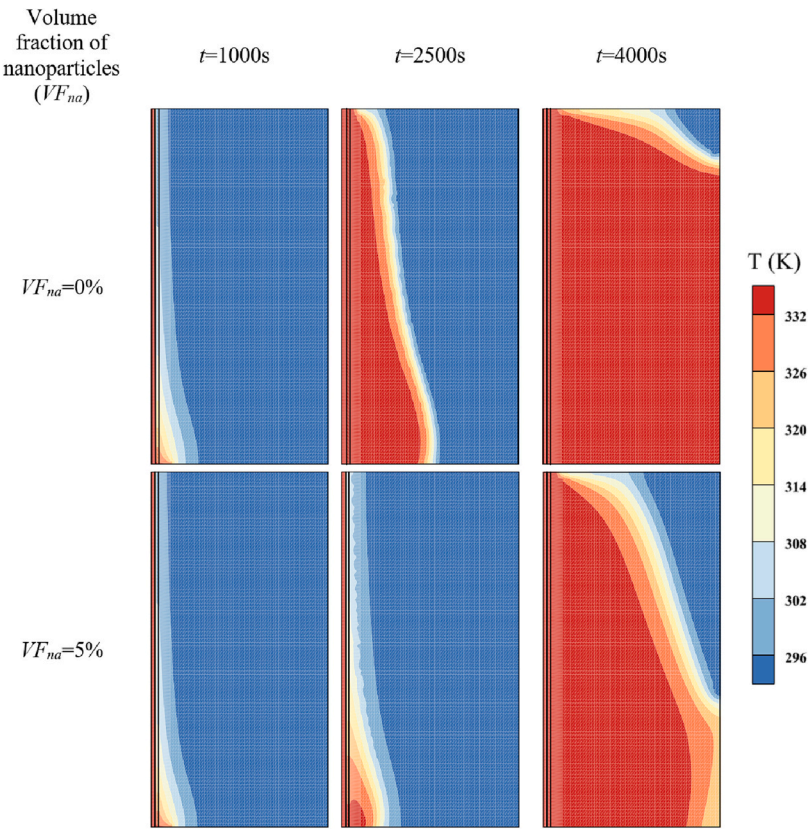

Fig. 16. Effect of volume fraction of the nanoparticles on the contour of isotherms; (Top row) $VF_{na} = 0$ % and (Bottom row) $VF_{na} = 5$ %, in the three different times.

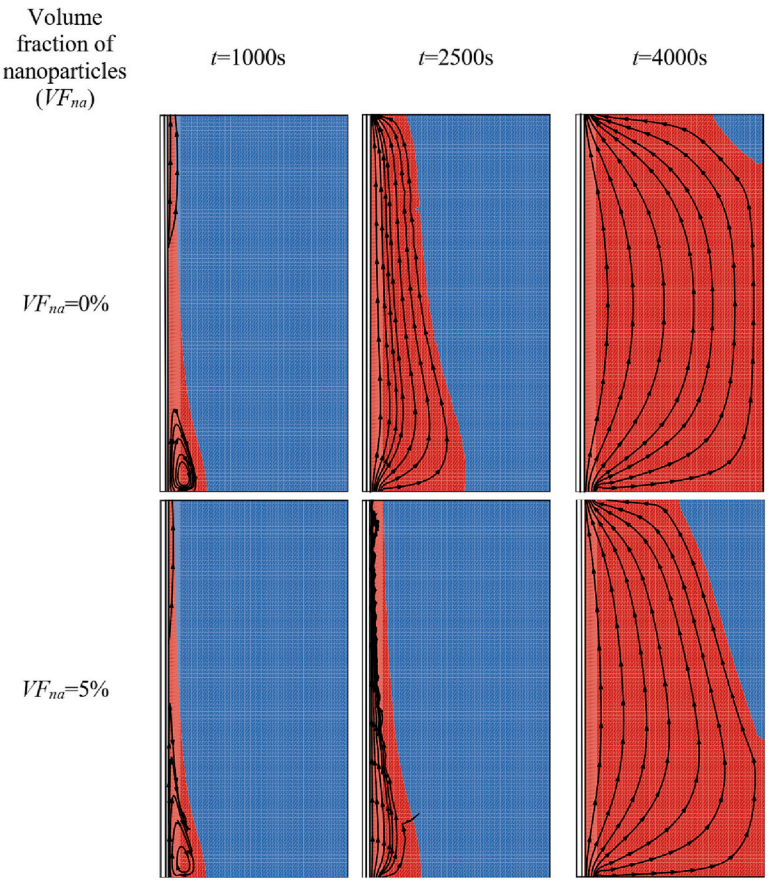

Fig. 17. Effect of volume fraction of the nanoparticles on the streamlines; (Top row) $VF_{na} = 0$ %, and (Bottom row) $VF_{na} = 5$ %, in the three different times.

Data availability statement

No data was used for the research described in the article.

CRediT authorship contribution statement

Mehdi Ghalambaz: Conceptualization, Methodology, Software, Validation, Formal analysis, Data Curation. **M. Aljaghtham:** Visualization, Original draft preparation, Investigation. Formal analysis, Data Curation. **M.A. Fteiti:** Methodology, Software; Formal analysis, Data Curation. **A.J. Chamkha:** Visualization, Original draft preparation, Investigation. Formal analysis, Data Curation. **A. Abdullah:** Methodology, Software; Formal analysis, Data Curation. **Mohammad Ghalambaz:** Investigation, Writing - Review & Editing, Supervision.

Declaration of competing interest

The authors clarify that there is no conflict of interest for report.

Data availability

No data was used for the research described in the article.

Acknowledgments

The authors extend their appreciation to the Deputyship for Research & Innovation, Ministry of Education in Saudi Arabia, for funding this research work through project number (IF-PSAU-2021/01/18928).

References

[1] S.A.M. Mehryan, M. Ghalambaz, L. Sasani Gargari, A. Hajjar, M. Sheremet, Natural convection flow of a suspension containing nano-encapsulated phase change particles in an eccentric annulus, J. Energy Storage 28 (2020).
[2] M. Ghalambaz, J.M. Mahdi, A. Shafaghat, A.H. Eisapour, O. Younis, P. Talebizadeh Sardari, W. Yaïci, Effect of twisted fin array in a triple-tube latent heat storage system during the charging mode, Sustainability 13 (5) (2021).
[3] T.H. Wang, T.-F. Yang, C.-H. Kao, W.-M. Yan, M. Ghalambaz, Paraffin core-polymer shell micro-encapsulated phase change materials and expanded graphite particles as an enhanced energy storage medium in heat exchangers, Adv. Powder Technol. 31 (6) (2020) 2421–2429.
[4] H. Nazir, M. Batool, F.J. Bolivar Osorio, M. Isaza-Ruiz, X. Xu, K. Vignarooban, P. Phelan, A.M.Kannan Inamuddin, Recent developments in phase change materials for energy storage applications: a review, Int. J. Heat Mass Transf. 129 (2019) 491–523.
[5] Y.B. Tao, Y.-L. He, A review of phase change material and performance enhancement method for latent heat storage system, Renew. Sust. Energ. Rev. 93 (2018) 245–259.
[6] S. Ushak, A. Gutierrez, H. Galleguillos, A.G. Fernandez, L.F. Cabeza, M. Grágeda, Thermophysical characterization of a by-product from the non-metallic industry as inorganic PCM, Sol. Energy Mater. Sol. Cells 132 (2015) 385–391.
[7] S. Ushak, A. Gutierrez, Y. Galazutdinova, C. Barreneche, L.F. Cabeza, M. Grágeda, Influence of alkaline chlorides on thermal energy storage properties of bischofite, Int. J. Energy Res. 40 (11) (2016) 1556–1563.
[8] W.-B. Ye, C. Li, S.-M. Huang, Y. Hong, Validation of thermal modeling of unsteady heat source generated in a rectangular lithium-ion power battery, Heat Transf. Res. 50 (3) (2019).
[9] W.-B. Ye, C. Li, S. Gong, Y. Hong, S.-M. Huang, S. Xu, Study on thermal uniformity and improvement for the drying of lithium-ion batteries, Int. J. Fluid Mech. Res. 46 (6) (2019).
[10] J. Luo, D. Zou, Y. Wang, S. Wang, L. Huang, Battery thermal management systems (BTMs) based on phase change material (PCM): a comprehensive review, Chem. Eng. J. 430 (2022), 132741.
[11] M. Ghalambaz, S.A.M. Mehryan, A. Tahmasebi, A. Hajjar, Non-Newtonian phase-change heat transfer of nano-enhanced octadecane with mesoporous silica particles in a tilted enclosure using a deformed mesh technique, Appl. Math. Model. 85 (2020) 318–337.
[12] J. Pereira da Cunha, P. Eames, Thermal energy storage for low and medium temperature applications using phase change materials – a review, Appl. Energy 177 (2016) 227–238.
[13] M. Esapour, M.J. Hosseini, A.A. Ranjbar, R. Bahrampoury, Numerical study on geometrical specifications and operational parameters of multi-tube heat storage systems, Appl. Therm. Eng. 109 (2016) 351–363.
[14] B. Praveen, S. Suresh, Thermal performance of micro-encapsulated PCM with LMA thermal percolation in TES based heat sink application, Energy Convers. Manag. 185 (2019) 75–86.
[15] A. Shahsavar, A. Shaham, P. Talebizadehsardari, Wavy channels triple-tube LHS unit with sinusoidal variable wavelength in charging/discharging mechanism, Int. Commun. Heat Mass Transfer 107 (2019) 93–105.
[16] A. Farzanehnia, M. Khatibi, M. Sardarabadi, M. Passandideh-Fard, Experimental investigation of multiwall carbon nanotube/paraffin based heat sink for electronic device thermal management, Energy Convers. Manag. 179 (2019) 314–325.
[17] M. Esapour, A. Hamzehnezhad, A.A. Rabienataj Darzi, M. Jourabian, Melting and solidification of PCM embedded in porous metal foam in horizontal multi-tube heat storage system, Energy Convers. Manag. 171 (2018) 398–410.
[18] P.T. Sardari, H.I. Mohammed, D. Giddings, G.S. Walker, M. Gillott, D. Grant, Numerical study of a multiple-segment metal foam-PCM latent heat storage unit: effect of porosity, pore density and location of heat source, Energy 189 (2019).
[19] W.T. Yan, C. Li, W.B. Ye, Numerical investigation of hydrodynamic and heat transfer performances of nanofluids in a fractal microchannel heat sink, heat Transfer—AsianResearch 48 (6) (2019) 2329–2349.
[20] W.T. Yan, W.B. Ye, C. Li, Effect of aspect ratio on saturated boiling flow in microchannels with nonuniform heat flux, heat Transfer—AsianResearch 48 (7) (2019) 3312–3327.
[21] N.H.S. Tay, M. Liu, M. Belusko, F. Bruno, Review on transportable phase change material in thermal energy storage systems, Renew. Sust. Energ. Rev. 75 (2017) 264–277.
[22] Y. Kozak, T. Rozenfeld, G. Ziskind, Close-contact melting in vertical annular enclosures with a non-isothermal base: theoretical modeling and application to thermal storage, Int. J. Heat Mass Transf. 72 (2014) 114–127.
[23] J.J. Vadasz, J.P. Meyer, S. Govender, G. Ziskind, Experimental study of vibration effects on heat transfer during solidification of paraffin in a spherical Shell, Exp. Heat Transfer 29 (3) (2015) 285–298.
[24] F. Hu, D.-W. Sun, W. Gao, Z. Zhang, X. Zeng, Z. Han, Effects of pre-existing bubbles on ice nucleation and crystallization during ultrasound-assisted freezing of water and sucrose solution, Innovative Food Sci. Emerg. Technol. 20 (2013) 161–166.
[25] V. Zipf, A. Neuhäuser, D. Willert, P. Nitz, S. Gschwander, W. Platzer, High temperature latent heat storage with a screw heat exchanger: design of prototype, Appl. Energy 109 (2013) 462–469.
[26] J. Gasia, D. Groulx, N.H.S. Tay, L.F. Cabeza, Numerical study of dynamic melting enhancement in a latent heat thermal energy storage system, J. Energy Storage 31 (2020).
[27] N.H.S. Tay, M. Belusko, M. Liu, F. Bruno, Investigation of the effect of dynamic melting in a tube-in-tank PCM system using a CFD model, Appl. Energy 137 (2015) 738–747.
[28] N.H.S. Tay, F. Bruno, M. Belusko, Experimental investigation of dynamic melting in a tube-in-tank PCM system, Appl. Energy 104 (2013) 137–148.
[29] B. He, F. Setterwall, Technical grade paraffin waxes as phase change materials for cool thermal storage and cool storage systems capital cost estimation, Energy Convers. Manag. 43 (13) (2002) 1709–1723.
[30] H.I. Mohammed, P.T. Sardari, D. Giddings, Multiphase flow and boiling heat transfer modelling of nanofluids in horizontal tubes embedded in a metal foam, International Journal of Thermal Sciences 146 (2019).
[31] P. Zhang, Z.N. Meng, H. Zhu, Y.L. Wang, S.P. Peng, Melting heat transfer characteristics of a composite phase change material fabricated by paraffin and metal foam, Appl. Energy 185 (2017) 1971–1983.
[32] P.T. Sardari, D. Grant, D. Giddings, G.S. Walker, M. Gillott, Composite metal foam/PCM energy store design for dwelling space air heating, Energy Convers. Manag. 201 (2019).
[33] Z. Liu, Y. Yao, H. Wu, Numerical modeling for solid–liquid phase change phenomena in porous media: Shell-and-tube type latent heat thermal energy storage, Appl. Energy 112 (2013) 1222–1232.
[34] X. Xiao, P. Zhang, M. Li, Preparation and thermal characterization of paraffin/metal foam composite phase change material, Appl. Energy 112 (2013) 1357–1366.
[35] R. Hossain, S. Mahmud, A. Dutta, I. Pop, Energy storage system based on nanoparticle-enhanced phase change material inside porous medium, Int. J. Therm. Sci. 91 (2015) 49–58.
[36] H. Zheng, C. Wang, Q. Liu, Z. Tian, X. Fan, Thermal performance of copper foam/paraffin composite phase change material, Energy Convers. Manag. 157 (2018) 372–381.
[37] S. Sivasankaran, A.I. Alsabery, I. Hashim, Internal heat generation effect on transient natural convection in a nanofluid-saturated local thermal non-equilibrium porous inclined cavity, Physica A 509 (2018) 275–293.
[38] P. Talebizadeh Sardari, G.S. Walker, M. Gillott, D. Grant, D. Giddings, Numerical modelling of phase change material melting process embedded in porous media: effect of heat storage size, Proc. Inst. Mech. Eng. A: J. Power Energy 234 (3) (2019) 365–383.
[39] J. Du, Y. Hong, S. Wang, W.-B. Ye, S.-M. Huang, Experimental thermal and flow characteristics in a traverse corrugated tube fitted with regularly spaced modified wire coils, Int. J. Therm. Sci. 133 (2018) 330–340.
[40] Y. Hong, J. Du, S. Wang, W.-B. Ye, S.-M. Huang, Turbulent thermal-hydraulic and thermodynamic characteristics in a traverse corrugated tube fitted with twin and triple wire coils, Int. J. Heat Mass Transf. 130 (2019) 483–495.
[41] D.A. Nield, A. Bejan, Convection in Porous Media, Springer Science & Business Media, 2006.
[42] J. Buongiorno, Convective transport in nanofluids, J. Heat Transf. 128 (3) (2006) 240–250.
[43] M. Sheikholeslami, M. Shamlooei, R. Moradi, Fe3O4-ethylene glycol nanofluid forced convection inside a porous enclosure in existence of coulomb force, J. Mol. Liq. 249 (2018) 429–437.

[44] J.M. Mahdi, E.C. Nsofor, Melting enhancement in triplex-tube latent heat energy storage system using nanoparticles-metal foam combination, Appl. Energy 191 (2017) 22–34.
[45] M. Al-Jethelah, S. Ebadi, K. Venkateshwar, S.H. Tasnim, S. Mahmud, A. Dutta, Charging nanoparticle enhanced bio-based PCM in open cell metallic foams: an experimental investigation, Appl. Therm. Eng. 148 (2019) 1029–1042.
[46] S.-K. Choi, S.-O. Kim, T.-H. Lee, Dohee-hahn, computation of the natural convection of nanofluid in a square cavity with homogeneous and nonhomogeneous models, Numer. Heat Transf.; A: Appl. 65 (4) (2014) 287–301.
[47] B. Kamkari, H. Shokouhmand, F. Bruno, Experimental investigation of the effect of inclination angle on convection-driven melting of phase change material in a rectangular enclosure, Int. J. Heat Mass Transf. 72 (2014) 186–200.
[48] M. Ghalambaz, S.A.M. Mehryan, K.A. Ayoubloo, A. Hajjar, M. El Kadri, O. Younis, M.S. Pour, C. Hulme-Smith, Thermal energy storage and heat transfer of Nano-enhanced phase change material (NePCM) in a Shell and tube thermal energy storage (TES) unit with a partial layer of eccentric copper foam, Molecules 26 (5) (2021) 1491.